INORGANIC CHEMISTRY FRONTIERS

RESEARCH ARTICLE

View Article Online
View Journal | View Issue

Cite this: *Inorg. Chem. Front.*, 2020, **7**, 4580

Luminescent Ir(III)–Ln(III) coordination polymers showing slow magnetization relaxation†

Kun Fan,[a] Song-Song Bao,[a] Ran Huo,[a] Xin-Da Huang,[a] Yu-Jie Liu,[a] Zi-Wen Yu,[a] Mohamedally Kurmoo[b] and Li-Min Zheng *[a]

Received 20th November 2019,
Accepted 13th January 2020

DOI: 10.1039/c9qi01504c

rsc.li/frontiers-inorganic

A series of iridium(III)–lanthanide(III) bimetallic coordination polymers were successfully obtained by hydrothermal reactions based on the Ir unit [Ir(ppy)$_2$(Hdcbpy)], namely, [Ln{Ir(ppy)$_2$(dcbpy)}$_2$(NO$_3$)(H$_2$O)$_n$]·solvent (**Ir$_2$Ln**, n = 5, Ln = Gd and Dy; and n = 4, Ln = Er and Yb) and [Ln$_2$(OH){Ir(ppy)$_2$(dcbpy)}$_4$(NO$_3$)(H$_2$O)$_4$]·solvent (**Ir$_4$Ln$_2$**, Ln = Gd, Dy, Er, and Yb). Compounds **Ir$_2$Ln** show chain structures in which the lanthanide ions are bridged by the Ir(ppy)$_2$(dcbpy)$^-$ ligands through the carboxylate groups. Compounds **Ir$_4$Ln$_2$** have double-chain structures, in which the dimers of Yb$_2$(OH) are connected by the Ir(ppy)$_2$(dcbpy)$^-$ ligands. Magnetic studies reveal that **Ir$_2$Dy** and **Ir$_4$Dy$_2$** exhibit slow magnetic relaxation behaviour in zero dc field, which is characteristic of single molecule magnets, but **Ir$_2$Er**, **Ir$_4$Yb$_2$**, **Ir$_4$Er$_2$** and **Ir$_4$Yb$_2$** require a field to induce such characteristics. Moreover, since the iridium(III) moiety can serve as an "antenna" to effectively sensitize the f–f transitions of the lanthanide ions, near-infrared luminescence has been observed for the Yb^{III} and Er^{III} complexes. As far as we know, this is the first observation of SMM behaviour and NIR luminescence in iridium(III)–lanthanide(III) bimetallic coordination polymers.

Introduction

The exponential growth of studies related to multifunctional coordination polymers integrating several physical and chemical properties into one single crystalline structure has become a hot topic of research over the last two decades.[1] Magnetoluminescent molecular materials belong to one family of those multifunctional materials which are gaining increasing attention due to their potential applications in several areas such as quantum computing, medical imaging and sensors.[2,3] One of the most effective strategies to combine magnetism with luminescence is the synthesis of lanthanide complexes which exhibit not only large unquenched orbital angular momentum and strong spin–orbit coupling that are ideal for the construction of single-molecule magnets (SMMs),[4,5] but also excellent luminescence properties including narrow line-like emission, high quantum yield and long lifetime.[2,6] Since the direct excitation of a lanthanide ion requires a Laporte forbidden f–f transition, indirect excitation *via* light-harvesting antennas or sensitizing chromophores is generally employed.[7] In comparison with the traditional organic chromophores being used as sensitizing groups,[8] using transition metal complexes allows more design flexibility, offering longer emission lifetime and extends the optical excitation window to lower energy region.[9] Their promising characteristics have therefore attracted substantial attention in recent years. Lanthanide ions that are near-infrared (NIR) emitters (Nd^{III}, Yb^{III}, Er^{III}, and Pr^{III}) have been involved in most of the work in this area and are useful in optical communication, medical imaging and biological labelling.[9,10]

Among the transition metals, the Ir^{III} complexes with energy levels modifiable through the cyclometalated ligands stand out as sensitizers for NIR emission from lanthanide ions.[11] The advantage is that the excitation is done in the visible region of the spectrum instead of the destructive UV light normally needed for organics. In 2008, De Cola and coworkers first reported a tetrametallic iridium–ytterbium complex showing NIR emission from Yb sensitized by the Ir complex.[12] Since then, several Ir^{III}–Ln^{III} bimetallic complexes showing NIR emission have been reported.[13] Furthermore, only three Ir^{III}–Ln^{III} (Ln = Yb, Er, and Nd) coordination polymers exhibiting NIR luminescence were reported by Luo *et al.* in 2014, which successfully extended the dimension of luminescent Ir^{III}–Ln^{III} system.[14]

[a]*State Key Laboratory of Coordination Chemistry, Coordination Chemistry Institute, School of Chemistry and Chemical Engineering, Collaborative Innovation Center of Advanced Microstructures, Nanjing University, Nanjing 210023, P. R. China. E-mail: lmzheng@nju.edu.cn*

[b]*Institut de Chimie, Université de Strasbourg CNRS-UMR7177, 4 rue Blaise Pascal, Strasbourg Cedex 67007, France*

†Electronic supplementary information (ESI) available: Synthetic details, structural data, IR, PXRD, TG. CCDC 1956646–1956649. For ESI and crystallographic data in CIF or other electronic format see DOI: 10.1039/c9qi01504c

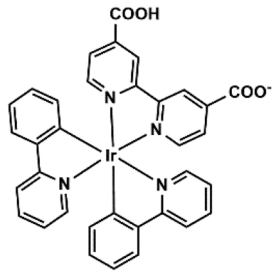

Scheme 1 The molecular structure of the metalloligand Ir(ppy)$_2$(Hdcbpy).

On the contrary, luminescent Ir^{III}–Ln^{III} single molecule magnets (SMMs) have been scarcely described. The only examples, as far as we are aware, are Ir$_6$Ln (Ln = Dy, Er, and Yb) clusters which have been reported by us and exhibit simultaneously slow magnetization relaxation from Ln^{III} and luminescence dominated by Ir^{III}.[15] However, no efficient energy transfer between Ir and Ln was observed.

Owing to our long-term interest in magneto-optical bifunctional materials,[15,16] herein we report two new series of Ir^{III}–Ln^{III} coordination polymers based on the metalloligand Ir(ppy)$_2$(Hdcbpy) (Scheme 1), namely, [Ln{Ir(ppy)$_2$(dcbpy)}$_2$(NO$_3$)(H$_2$O)$_n$]·solvent (**Ir$_2$Ln**, n = 5, Ln = Gd and Dy; and n = 4, Ln = Er and Yb) and [Ln$_2$(OH){Ir(ppy)$_2$(dcbpy)}$_4$(NO$_3$)(H$_2$O)$_4$]·solvent (**Ir$_4$Ln$_2$**, Ln = Gd, Dy, Er, and Yb). **Ir$_2$Ln** show chain structures, in which the Ln^{III} ions are cross-linked by the Ir(ppy)$_2$(dcbpy)$^-$ ligands *via* the two carboxylate groups. For **Ir$_4$Ln$_2$**, dimers of Ln$_2$(OH) are observed, which are further connected by the carboxylate groups of the Ir(ppy)$_2$(dcbpy)$^-$ ligands, forming a ladder-like chain structure. Interestingly, both single molecule magnetism and Ir → Ln energy transfer accompanied by near-infrared emission were demonstrated to co-exist in **Ir$_2$Ln** and **Ir$_4$Ln$_2$** (Ln = Er and Yb).

Results and discussion

Crystal structures

Compounds [Ln{Ir(ppy)$_2$(dcbpy)}$_2$(NO$_3$)(H$_2$O)$_n$]·solvent (**Ir$_2$Ln**, n = 5, Ln = Gd and Dy; and n = 4, Ln = Er and Yb) and [Ln$_2$(OH) {Ir(ppy)$_2$(dcbpy)}$_4$(NO$_3$)(H$_2$O)$_4$]·solvent (**Ir$_4$Ln$_2$**, Ln = Gd, Dy, Er, and Yb) were synthesized by solvothermal reactions of Ir(ppy)$_2$(Hdcbpy) and Ln(NO$_3$)$_3$·6H$_2$O in H$_2$O/MeOH using different concentrations of NaOH and temperatures. Powder XRD measurements revealed that **Ir$_2$Ln** (Ln = Gd, Dy, Er, and Yb) and **Ir$_4$Ln$_2$** (Ln = Gd, Dy, Er, and Yb) are isostructural compounds. However, single crystals of good quality were obtained only for compounds **Ir$_2$Dy**, **Ir$_2$Er**, **Ir$_2$Yb** and **Ir$_4$Yb$_2$**. The crystallographic data for these four compounds are given in Table 1.

Ir$_2$Ln are isomorphous compounds that crystallize in the triclinic $P\bar{1}$ space group, though the numbers of the coordination water molecules are slightly different (n = 5 for Ln = Gd and Dy; and n = 4 for Ln = Er and Yb). Therefore, **Ir$_2$Yb** is selected as a representative for the description of the structures. The asymmetric unit of **Ir$_2$Yb** consists of two Ir(ppy)$_2$(dcbpy)$^-$ ligands, one Yb^{III}, one NO$_3^-$, four coordinated water molecules, two MeOH and 0.5 lattice water molecule. As shown in Fig. 1a and b, the Yb atom is seven-coordinated by three carboxylate oxygen atoms from three ligands (O1, O3A, and O5) and four coordination water molecules. One of the coordination water molecules is disordered over two sites (O4W and O4W′) (Fig. 1b). Continuous Shape Measure (CShM) analysis[17] suggests that the geometries of the two possible

Table 1 Crystallographic data for compounds **Ir$_2$Dy**, **Ir$_2$Er**, **Ir$_2$Yb** and **Ir$_4$Yb$_2$**

	Ir$_2$Dy	**Ir$_2$Er**	**Ir$_2$Yb**	**Ir$_4$Yb$_2$**
Formula	$C_{68}H_{54}N_8O_{13}DyIr_2$	$C_{140}H_{122}N_{18}O_{35}Er_2Ir_4$	$C_{140}H_{122}N_{18}O_{35}Yb_2Ir_4$	$C_{280}H_{236}N_{34}O_{61}Yb_4Ir_8$
M	1738.09	3719.87	3731.43	7282.77
Crystal system	Triclinic	Triclinic	Triclinic	Monoclinic
Space group	$P\bar{1}$	$P\bar{1}$	$P\bar{1}$	$P2_1/c$
a (Å)	8.5559(13)	8.6129(14)	8.5775(16)	36.569(3)
b (Å)	18.370(3)	18.343(3)	18.360(3)	8.6347(5)
c (Å)	23.830(4)	23.903(4)	23.823(4)	43.991(3)
α (°)	70.638(3)	70.841(4)	70.887(5)	90
β (°)	80.107(3)	80.828(4)	81.179(6)	112.317(2)
γ (°)	77.866(3)	77.440(3)	77.676(5)	90
V (Å^3)	3433.3(9)	3465.9(10)	3449.0(11)	12 850.4(14)
Z	2	1	1	2
ρ_{calcd} (g cm^{-3})	1.681	1.782	1.797	1.882
μ (mm^{-1})	5.009	5.106	5.270	5.653
F (000)	1684.0	1812.0	1816.0	7076.0
R_{int}	0.0495	0.0482	0.0432	0.0617
T_{max}, T_{min}	0.634, 0.350	0.629, 0.350	0.621, 0.350	0.728, 0.360
R_1 [a], wR_2 [b] [$I > 2\sigma(I)$]	0.1105, 0.2755	0.0795, 0.1847	0.0485, 0.1178	0.0844, 0.1952
R_1 [a], wR_2 [b] (all data)	0.1273, 0.2852	0.1093, 0.2019	0.0621, 0.1244	0.1012, 0.2036
GoF on F^2	1.110	1.031	0.998	1.022
$(\Delta\rho)_{max}$, $(\Delta\rho)_{min}$ (e Å^{-3})	5.05, −8.18	4.86, −6.94	2.22, −1.97	5.32, −3.22
CCDC	1956646	1956647	1956648	1956649

[a] $R_1 = \sum||F_o| - |F_c||/\sum|F_o|$. [b] $wR_2 = [\sum w(F_o^2 - F_c^2)^2/\sum w(F_o^2)^2]^{1/2}$.

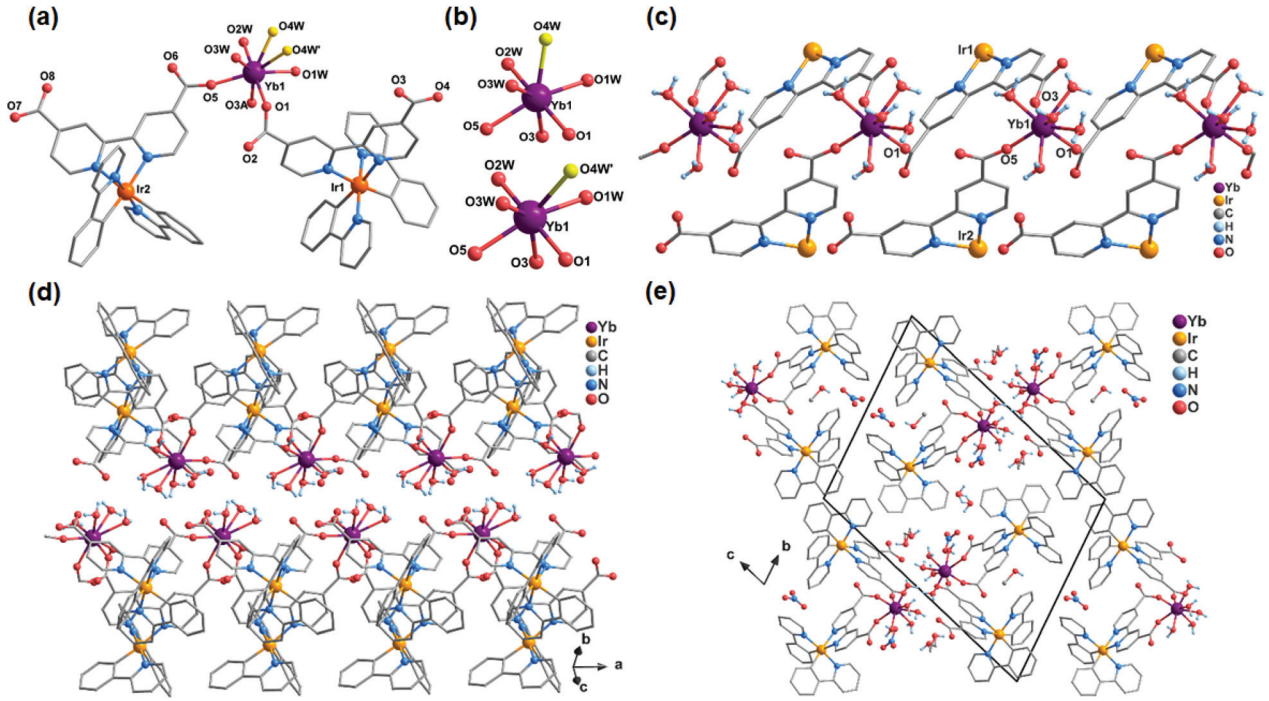

Fig. 1 (a) The building unit of the structure of Ir_2Yb. (b) Coordination environments of the Yb^{III} ion. (c) The single chain structure of the compound Ir_2Yb. The ppy ligands are omitted for clarity. (d) The double-chain structure of Ir_2Yb. (e) Packing diagram of the structure of Ir_2Yb viewed along the *a*-axis. All H atoms except those attached to the oxygen atoms are omitted for clarity.

$[YbO_7]$ polyhedra are slightly deviated from an ideal capped trigonal prism (CShM = 1.17) and pentagonal bipyramid (CShM = 1.25), respectively. The Yb–O bond lengths are in the range of 2.191(7)–2.452(18) Å, and the O–Yb–O angles are in the range of 67.4(5)–149.8(3)°.

Two $Ir(ppy)_2(dcbpy)^-$ ligands are crystallographically distinguished. One ligand (Ir1) adopts a bi-dentate coordination mode by using two of its four carboxylate oxygen atoms (O1 and O3), and connects the neighbouring Yb centres into an infinite chain running along the *a*-axis. The other ligand (Ir2) adopts a mono-dentate coordination mode and binds the Yb atom through its carboxylate oxygen atom O5 (Fig. 1c). The Yb···Yb distance within the chain is 8.58 Å. The chain is polar with the $Ir(ppy)_2(dcbpy)^-$ ligands sitting on one side and the coordination water molecules on the other side. Two equivalent chains are connected through extensive hydrogen bonding interactions between the coordination water molecules, forming a supramolecular double chain which is non-polar (Fig. 1d). The shortest interchain Yb···Yb separation is 6.20 Å. The double chains are stacked along the *a*-axis with the space between the double-chains filled with lattice water and methanol molecules and nitrate anions (Fig. 1e). Extensive H-bonds are observed among the aromatic groups, the non-coordinated carboxylate oxygen atoms, the coordination and lattice water molecules and the nitrate anions. A three-dimensional supramolecular network is thus constructed.

Compounds Ir_2Dy and Ir_2Er show similar 3D supramolecular structures made up of 1D chain (Fig. S3 and S4†). However, a significant difference is found in the coordination environment of Dy^{III} in Ir_2Dy. Unlike the seven-coordinated lanthanide ion in Ir_2Yb and Ir_2Er (Fig. S4†), the Dy atom is eight-coordinated by three carboxylate oxygen atoms from three ligands (O1, O3A, and O5) [Dy–O: 2.270(16)–2.376(16) Å] and five coordinated water molecules (O1W, O2W, O3W, O4W, and O5W) [Dy–O: 2.332(19)–2.48(3) Å] (Fig. 2). This can be related to the lanthanide contract effect, the Dy^{III} ion with larger ionic radius shows higher coordination number. The geometry of Dy^{III} is best described as a slightly distorted triangular dodecahedron (D_{2d}) with a CShM value of 0.94.

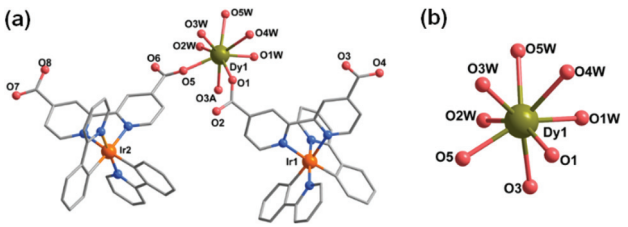

Fig. 2 (a) The building unit of the structure of Ir_2Dy. (b) The coordination environment of the Dy^{III} ion.

The compound Ir_4Yb_2 crystallizes in the monoclinic space group $P2_1/c$. Its asymmetric unit contains four $Ir(ppy)_2(dcbpy)^-$ ligands, two Yb^{III}, one OH^-, one NO_3^-, four coordinated water molecules, four free MeOH molecules and two and a half lattice water molecules. As shown in Fig. 3, both the crystallographically distinct Yb atoms have seven coordinated environments, *viz*. four carboxylate oxygen atoms, one bridging co-

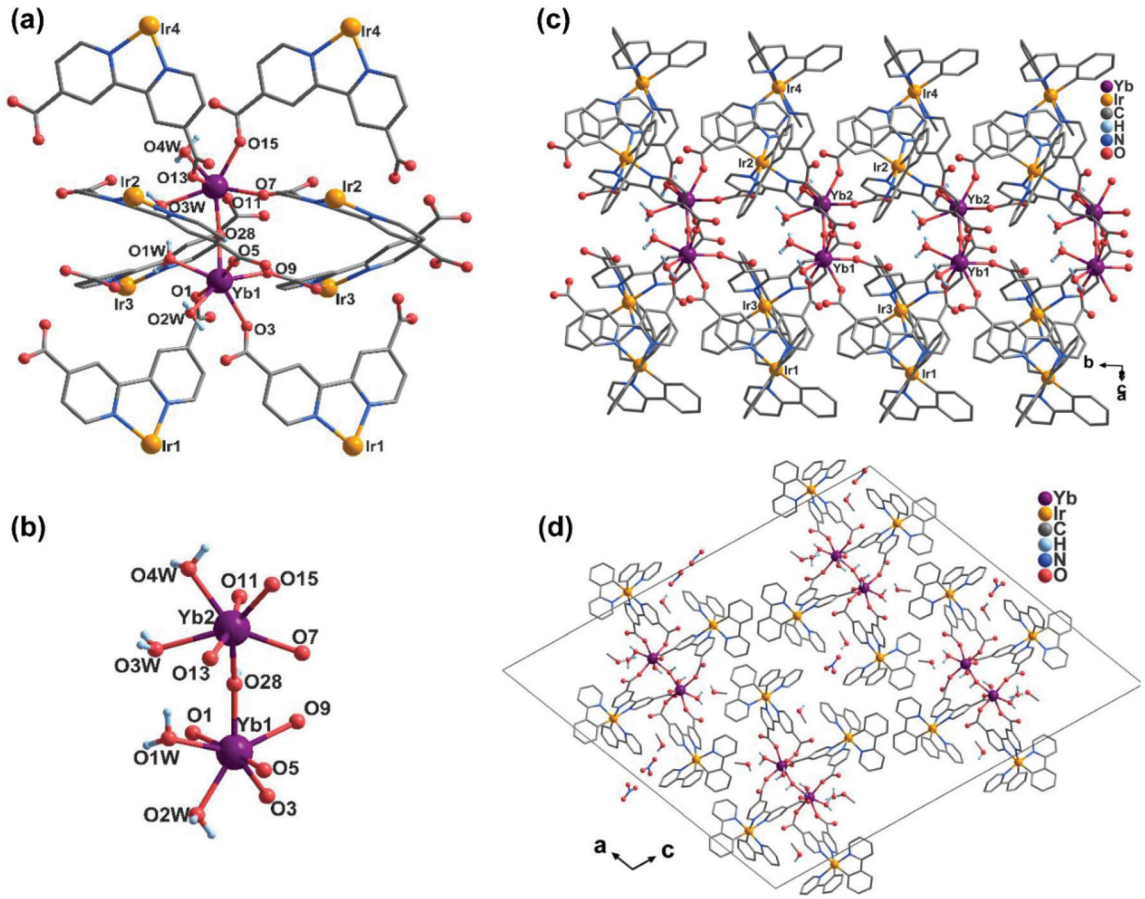

Fig. 3 (a) The building unit of the structure of Ir_4Yb_2. The ppy ligands are omitted for clarity. (b) Coordination environments of the Yb^{III} ions. (c) The double-chain structure of the compound Ir_4Yb_2. (d) Packing diagram of the structure of Ir_4Yb_2 viewed along the *b*-axis. All H atoms except those attached to the oxygen atoms are omitted for clarity.

ordinated OH^- and two oxygen atoms from water (Fig. 3b). Both Yb^{III} ions adopt pentagonal bipyramidal geometry, as suggested by the CShM values $S(D_{5h})$ = 1.80 (Yb1) and $S(D_{5h})$ = 0.96 (Yb2). The neighbouring [YbO_7] polyhedra are linked *via* the OH^- group, forming a dimer of $\{Yb_2(OH)(COO)_8(H_2O)_4\}$ (Yb–O–Yb = 159.6(1)° and Yb···Yb = 4.3962(11) Å). All of the Ir $(ppy)_2(dcbpy)^-$ ligands adopt a bi-dentate coordination mode, unlike those in **Ir_2Ln**, and connect the $\{Yb_2(OH)(COO)_8(H_2O)_4\}$ dimers into a one-dimensional double-chain structure (Fig. 3c). The intrachain Yb···Yb distance between the dimers is 8.63 Å. The double chains are stacked in the lattice. The lattice solvent molecules and the nitrate anions occupy the inter-chain spaces, and are involved in the extensive H-bond network.

Although single crystals of good quality were not obtained for compounds **Ir_2Gd**, **Ir_4Gd_2**, **Ir_4Dy_2** and **Ir_4Er_2**, the unit cell parameters were confirmed by Pawley fitting of their powder diffraction patterns using TOPAS 5.0 program (Table S8, Fig. S5–S10†).

Obviously, the structure of **Ir_4Yb_2** is significantly different from that of **Ir_2Yb**. A careful analysis reveals, however, that the double chain in **Ir_4Yb_2** can be viewed as two single chains in **Ir_2Yb** connected by the hydroxyl groups. The involvement of an OH^- group in **Ir_4Yb_2** can be explained by the more basic reaction condition used for the synthesis of **Ir_4Yb_2**.

Notably, Ir^{III}–Ln^{III} coordination polymers containing the same ligand Ir(ppy)$_2$(Hdcbpy) are still rare. The only examples, as far as we are aware, are Ln[Ir(ppy)$_2$(dcbpy)]$_2$(OH)·H_2O (Ln = Gd, Yb, Er, and Nd)[14] and Y[Ir(ppy)$_2$(dcbpy)]$_2$(OH).[18] These compounds possess identical chain structures that are remarkably different from those of **Ir_2Yb** and **Ir_4Yb_2**, in which the dimers of edge-sharing $\{LnO_7\}$ or $\{YO_7\}$ pentagonal bipyramid *via* two OH^- groups are further connected by the carboxylate groups in the metalloligand. Therefore compounds **Ir_2Ln** and **Ir_4Ln_2** provide new structural types of the Ir^{III}–Ln^{III} coordination polymers based on Ir(ppy)$_2$(Hdcbpy).

Magnetic properties

Variable temperature dc magnetic susceptibilities of **Ir_2Ln** and **Ir_4Ln_2** (Ln = Gd, Dy, Er, and Yb) were measured in the temperature range of 2–300 K in an applied field of 1 kOe. Plots of $\chi_M T$ *versus* T (χ_M is the molar magnetic susceptibility per Ln^{III} ion) for these compounds are shown in Fig. 4. At 300 K, the $\chi_M T$ values are 7.73 and 7.84 cm^3 K mol^{-1} for **Ir_2Gd** and **Ir_4Gd_2**,

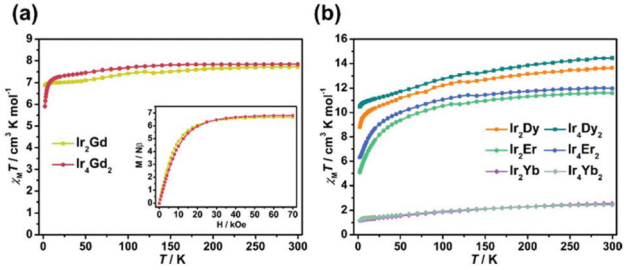

Fig. 4 (a) Temperature dependence of $\chi_M T$ per Gd on cooling in a field of 1 kOe for **Ir$_2$Gd** and **Ir$_4$Gd$_2$**. Inset: *M vs. H* plots of the two compounds at 2 K. (b) Temperature dependence of $\chi_M T$ per Ln on cooling in a field of 1 kOe for **Ir$_2$Ln** and **Ir$_4$Ln$_2$** (Ln = Dy, Er, and Yb).

respectively, which are close to the expected value of 7.88 cm^3 K mol^{-1} for an isolated Gd^{III} ion (S = 7/2, L = 0, $^8S_{7/2}$, J = 7/2, g = 2). Upon cooling, the $\chi_M T$ value of **Ir$_2$Gd** decreases continuously in the range of 300–50 K and then decreases smoothly to the minimum value of 6.88 cm^3 K mol^{-1} at 2 K. In contrast, for compound **Ir$_4$Gd$_2$**, the $\chi_M T$ value decreases to 20 K followed by a rapid drop to the minimum value of 5.91 cm^3 K mol^{-1} at 2 K. The low temperature feature could be attributed to the occurrence of the Gd^{III}···Gd^{III} antiferromagnetic exchange interactions, and is given by the negative values of the Weiss constants (θ) as −0.04 K for **Ir$_2$Gd** and −0.54 K for **Ir$_4$Gd$_2$** (Fig. S11†). The stronger antiferromagnetic interactions in **Ir$_4$Gd$_2$** may be due to short distances of the Gd^{III} ions in the dimer connected *via* the OH$^-$ group. The field dependence of the magnetization at 2 K shows a rapid increase at low field and then slowly reaches the corresponding maximum values of 6.67$N\beta$ per Gd for **Ir$_2$Gd** and 6.80$N\beta$ per Gd for **Ir$_4$Gd$_2$** at 70 kOe, which are close to the theoretical saturation value of 7$N\beta$ for an isolated Gd^{III} ion.

The dc magnetic susceptibilities of compounds **Ir$_2$Ln** and **Ir$_4$Ln$_2$** (Ln = Dy, Er, and Yb) were measured under the same conditions. As shown in Fig. 4b, all the compounds show a similar behaviour. The room temperature $\chi_M T$ values per Ln are 13.65 (**Ir$_2$Dy**), 14.44 (**Ir$_4$Dy$_2$**), 11.60 (**Ir$_2$Er**), 11.98 (**Ir$_4$Er$_2$**), 2.53 (**Ir$_2$Yb**) and 2.45 (**Ir$_4$Yb$_2$**) cm^3 K mol^{-1}, which are consistent with the theoretical values of 14.17 (Dy^{III}, $^6H_{15/2}$), 11.48 (Er^{III}, $^4I_{15/2}$) and 2.57 (Yb^{III}, $^2F_{7/2}$) cm^3 K mol^{-1}. The decrease in the $\chi_M T$ value on lowering the temperature is attributed to the thermal depopulation of the excited M_J sublevels and/or the weak antiferromagnetic exchange interactions between the metal centres.[19] The magnetization values of compounds **Ir$_2$Ln** and **Ir$_4$Ln$_2$** at 2 K and 70 kOe are significantly smaller than the expected saturation values for the corresponding lanthanide ions, revealing the existence of a significant magnetic anisotropy[20] which is further confirmed by the non-superimposed *M vs. H*/*T* plots at different temperatures (Fig. S12 and S13†).

In order to assess the effect of coordination configuration on the dynamic magnetic properties, the alternative-current (ac) magnetic susceptibilities of **Ir$_2$Ln** and **Ir$_4$Ln$_2$** (Ln = Dy, Er, and Yb) were measured using a Quantum Design PPMS in the frequency range of 10–10 000 Hz. Under the zero dc field, only

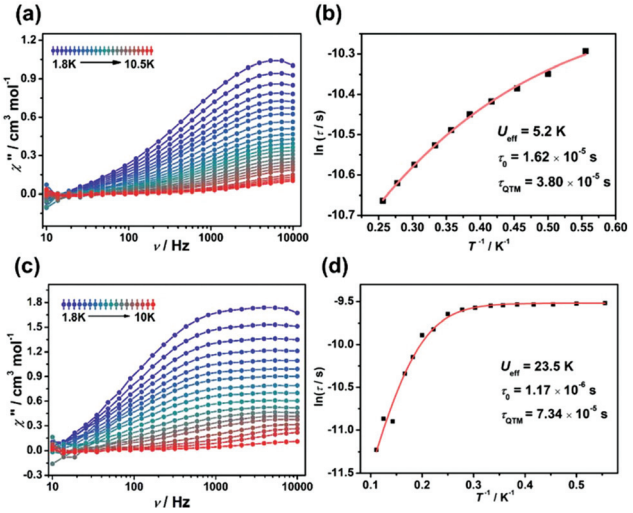

Fig. 5 Out-of-phase (χ'') ac susceptibilities of **Ir$_2$Dy** (a) and **Ir$_4$Dy$_2$** (c) under zero dc field. Plots of ln(τ) *vs.* 1/*T* for **Ir$_2$Dy** (b) and **Ir$_4$Dy$_2$** (d).

Ir$_2$Dy and **Ir$_4$Dy$_2$** showed clear frequency dependence of in-phase (χ') and out-of-phase (χ'') susceptibilities below *ca.* 11 K, indicating a zero-field SMM with slow magnetization relaxation (Fig. 5a and c). However, the peak value of χ'' did not change significantly with increasing temperature, indicating that the magnetic relaxation mainly originated from the quantum tunnelling process.[21] The Cole–Cole plots can be well fit by the generalized Debye model to extract the relaxation time (τ) (Tables S9 and S14†).[22] The distribution parameters (α) are in the range of 0.34–0.37 for **Ir$_2$Dy** and in the range of 0.25–0.45 for **Ir$_4$Dy$_2$**, suggesting multiple relaxation processes with broad distribution of the relaxation times. Moreover, the ln τ *vs.* T^{-1} curve can be fit by considering the Orbach and quantum tunnelling process using eqn (1), and determining the parameters U_{eff} = 5.2 K, $\tau_0 = 1.6 \times 10^{-5}$ s, and $\tau_{QTM} = 3.8 \times 10^{-5}$ s for **Ir$_2$Dy** (Fig. 5b), and U_{eff} = 23.5 K, $\tau_0 = 1.17 \times 10^{-6}$ s, and $\tau_{QTM} = 7.34 \times 10^{-4}$ s for **Ir$_4$Dy$_2$** (Fig. 5d), respectively.

$$\tau^{-1} = {\tau_{QTM}}^{-1} + {\tau_0}^{-1} \exp(-U_{eff}/kT) \quad (1)$$

$$\tau^{-1} = {\tau_{QTM}}^{-1} + AT + {\tau_0}^{-1} \exp(-U_{eff}/kT) \quad (2)$$

In order to suppress the QTM and get further insight into the magnetic relaxation dynamics of complexes **Ir$_2$Dy** and **Ir$_4$Dy$_2$**, we obtained the ac magnetic susceptibilities under an applied dc bias field of 2 kOe. Variable-frequency ac magnetic susceptibilities of **Ir$_2$Dy** are shown in Fig. S15 and S16.† With increasing temperature, the position of χ'' peak did not change below 5.4 K, indicating a complicated relaxation process. The Cole–Cole plots were generated using the frequency dependent ac susceptibilities in the temperature region of 5.4–7.5 K, and can be well fit by employing the sum of two modified Debye functions. For the fast relaxation (FR) process, the low value of the relaxation width ($\alpha_1 \approx 0$, Table S10†) suggests a narrow distribution of relaxation times, and the temperature

independence of ln τ also indicates that only the quantum tunnelling mechanism is involved.[24] However, the slow relaxation (SR) processes show a linear temperature dependence of ln τ corresponding to an Orbach relaxation mechanism,[25] leading to the parameters U_{eff} = 38.1 K and $\tau_0 = 2.93 \times 10^{-6}$ s according to the Arrhenius law (Fig. S16d†).

For compounds **Ir_4Dy_2**, the frequency-dependent χ'' exhibits more clear peaks than in zero-dc field and the positions of maxima change from high to low frequency as the temperature is decreased. Although there are two crystallographic sites differing in environments in **Ir_4Dy_2**, no dual magnetization relaxation processes were distinguished. It is possible to fit the Cole–Cole plots with only one relaxation process (Fig. S18 and 19, Table S12†).[26] Furthermore, the temperature dependent relaxation time profiles can be fit as a sum of the contributions of the Orbach, quantum tunnelling, and direct mechanisms (eqn (2)).[27] The best fit led to the following parameters: U_{eff} = 21.4 K, $\tau_0 = 2.89 \times 10^{-6}$ s, $\tau_{QTM} = 7.98 \times 10^{-4}$ s and A = 193.9 K^{-1} s^{-1}. Obviously, the parameters of Orbach and quantum tunnelling processes do not change significantly under an applied field, but the direct process induced by the applied field results in the decrease of the magnetic relaxation rate.

The magnetization dynamics of compounds **Ir_2Er** and **Ir_4Er_2** were also explored. Unfortunately, under zero external field, neither peaks nor frequency dependence of χ' and χ'' was found at 2 K, indicating the presence of significant QTM effect. When an external dc field was applied, both χ' and χ'' were found and they showed frequency-dependence, which are typical of a field-induced SMM behaviour (Fig. S20–S23, Tables S13 and S14†). As shown in Fig. S21 and S23,† the maximum of χ'' gradually shifted to high frequencies with increasing temperature, while no maximum was observed above 2.2 K. The relaxation time τ can be extracted by fitting the Cole–Cole plots using the generalized Debye model assuming a single relaxation process. The ln τ values increase linearly with temperature in the range of 1.8–2.6 K, and an Arrhenius law fitting results in the energy barriers of 13.6 K ($\tau_0 = 2.72 \times 10^{-8}$ s) for **Ir_2Er** and 11.8 K ($\tau_0 = 6.68 \times 10^{-8}$ s) for **Ir_4Er_2**.

The temperature-dependent magnetic dynamics of **Ir_2Yb** and **Ir_4Yb_2** were also investigated under an external dc field (Fig. 6, S24–S27, Tables S15 and S16†). For **Ir_2Yb**, the frequency scan of χ'' exhibited single peaks below 6 K and the maxima gradually shifted to high frequencies upon heating. By assuming a single relaxation process, the relaxation time τ can again be extracted by fitting the Cole–Cole plots using the generalized Debye model. The ln τ *vs.* T^{-1} curve can be reasonably fit by using eqn (2), leading to the parameters U_{eff} = 24.4 K, $\tau_0 = 2.88 \times 10^{-7}$ s, and A = 687.9 K^{-1} s^{-1}. However, two distinct peaks at low temperatures were observed in the temperature-dependent magnetic dynamics of **Ir_4Yb_2**, indicating dual relaxation processes by accounting for the different combinations of contributions from the direct and Orbach relaxation processes. The ln τ *vs.* T^{-1} profile can be fit in the whole temperature range,[28] and the resulting parameters are U_{eff} = 22.2 K, $\tau_0 = 2.03 \times 10^{-7}$ s and A = 8678 K^{-1} s^{-1} for the FR process, while U_{eff} = 28.3 K, $\tau_0 = 2.5 \times 10^{-8}$ s and A = 682 K^{-1} s^{-1} for the SR process. The observation of dual magnetization relaxation processes in **Ir_4Yb_2** could result from the presence of two crystallographic sites with two different environments in the structure.

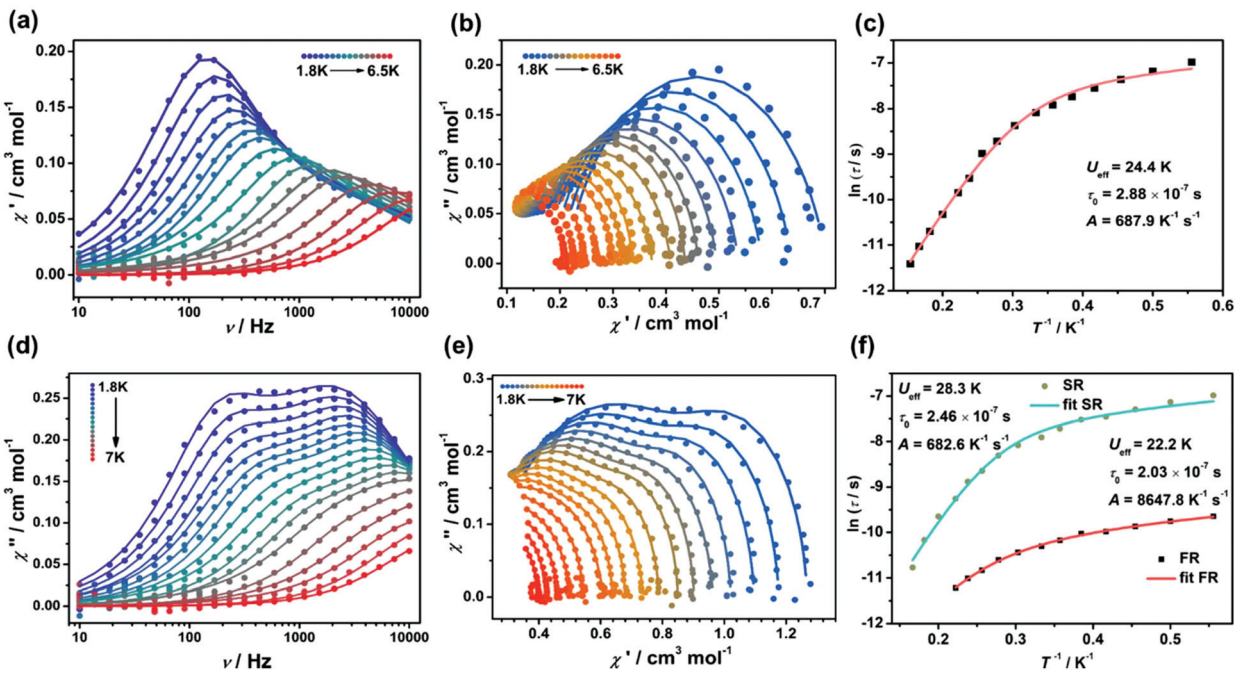

Fig. 6 Frequency dependence of out-of-phase (χ'') ac susceptibilities at different temperatures for **Ir_2Yb** (a) and **Ir_4Yb_2** (d) under an external dc field. The Cole–Cole plots of the ac susceptibilities for **Ir_2Yb** (b) and **Ir_4Yb_2** (e). Plots of ln(τ) *vs.* 1/T for **Ir_2Yb** (c) and **Ir_4Yb_2** (f).

A similar phenomenon was also observed in a few other Yb dimer complexes.[29]

To the benefit of the D_{5h} symmetry, especially the Kramers Dy^{III} and Er^{III} ions, the observation of high energy barrier to moment reversal in Ln–SMMs was reported by several groups.[30–32] Therefore, a small anisotropy barrier in Ir–Ln bimetallic complexes is not expected. This may be explained by the orientation of the easy-axis anisotropy deviating significantly from an idealized C_5 axis, which has been observed in other lanthanide complexes.[33]

Optical properties

The UV-vis spectra of the free metalloligand and Ir–Ln coordination polymers in the solid state were transformed from the diffuse reflectance spectra using the Kubelka–Munk equation: $F(R) = (1 - R)^2/2R$. As shown in Fig. S28,† the absorptions in the high energy region (250–330 nm) are associated with the π–π* transition of the aromatic ligands (Hdcbpy and ppy) and the intense absorption bands at 330–450 nm can be explained by the mixed spin-allowed ^{1}LLCT (ligand-to-ligand charge-transfer) and ^{1}MLCT (metal-to-ligand charge-transfer). The lower energy absorptions (*ca.* 450–550 nm) originate from the spin forbidden ^{3}MLCT and are common in cyclometalated iridium derivatives.[34] The absorption profiles of all Ir–Ln complexes show a similar electronic transition to the Ir^{III} unit. However, the most significant difference is that weak absorption peaks located at 755 nm (13 245 cm^{-1}) and 654 nm (15 290 cm^{-1}) were observed for **Ir_2Dy** and **Ir_2Er**, respectively, corresponding to the f–f transitions of the Dy^{III} ions ($^5H_{15/2}$ to $^6F_{3/2}$) and Er^{III} ions ($^4I_{15/2}$ to $^4F_{9/2}$).[35] Although the structures are different, a similar phenomenon was also observed for **Ir_4Dy_2** and **Ir_4Er_2**.

Upon excitation in the visible region at 375 nm, Ir(ppy)$_2$(Hdcbpy) exhibits a strong emission band at 605 nm, corresponding to the ^{3}MLCT transition as a consequence of the heavy-atom effect. As is to be expected, the solid-state luminescence spectra of compounds **Ir_2Ln** and **Ir_4Ln_2** (Ln = Gd, Dy, Er, and Yb) are similar to that of the free metalloligand, indicating that the phosphorescence of polymers arises from the Ir(III) unit (Fig. 7 and Table 2). However, the emission

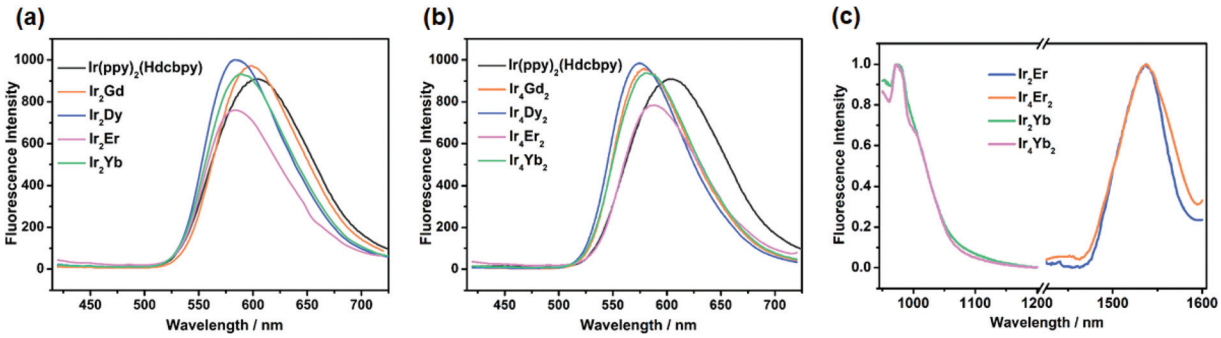

Fig. 7 (a) The emission spectra of Ir(ppy)$_2$(Hdcbpy) and **Ir_2Ln** in the solid-state (λ_{ex} = 375 nm). (b) The emission spectra of Ir(ppy)$_2$(Hdcbpy) and **Ir_4Ln_2** (Ln = Gd, Dy, Er, Yb) in the solid-state (λ_{ex} = 375 nm). (c) The solid-state NIR emission spectra of the Ir–Yb (left) and Ir–Er (right) complexes (λ_{ex} = 500 nm).

Table 2 Magnetic and photophysical parameters of **Ir_2Ln** and **Ir_4Ln_2** (Ln = Gd, Dy, Er, and Yb)

	dc field	Relaxation processes	Fitting parameters	λ_{em}/nm	τ/μs	QY/%
Ir(ppy)$_2$(Hdcbpy)	—	—	—	605	6.60	4.22
Ir_2Gd	—	—	—	598	8.69	5.83
Ir_4Gd_2	—	—	—	578	7.74	8.08
Ir_2Dy	0 kOe	Orbach, QTM	U_{eff} = 5.2 K, $\tau_0 = 1.62 \times 10^{-5}$ s, $\tau_{QTM} = 3.80 \times 10^{-5}$ s	583	4.79	6.00
	2.0 kOe	QTM (FR)	$\tau_{QTM} = 2.25 \times 10^{-5}$			
		Orbach(SR)	U_{eff} = 38.1 K, $\tau_0 = 2.93 \times 10^{-6}$ s			
Ir_4Dy_2	0 kOe	Orbach, QTM	U_{eff} = 23.5 K, $\tau_0 = 1.17 \times 10^{-6}$ s	575	0.66	11.94
			$\tau_{QTM} = 7.34 \times 10^{-4}$ s			
	2.0 kOe	Orbach, QTM;	U_{eff} = 21.4 K, $\tau_0 = 2.89 \times 10^{-6}$ s			
		direct	$\tau_{QTM} = 7.98 \times 10^{-4}$ s, A = 193.9 K^{-1} s^{-1}			
Ir_2Er	1.0 kOe	Orbach	U_{eff} = 13.6 K, $\tau_0 = 2.72 \times 10^{-8}$ s	584	6.37	0.68
				1538	1.40	—
Ir_4Er_2	1.5 kOe	Orbach	U_{eff} = 11.8 K, $\tau_0 = 6.68 \times 10^{-8}$ s	588	5.47	1.08
				1538	1.37	—
Ir_2Yb	1.0 kOe	Orbach, direct	U_{eff} = 24.4 k, $\tau_0 = 2.88 \times 10^{-7}$ s, A = 687.9 K^{-1} s^{-1}	590	2.23	5.60
				975	0.92	—
Ir_4Yb_2	1.5 kOe	Orbach, direct (FR)	U_{eff} = 22.2 K, $\tau_0 = 2.03 \times 10^{-7}$ s	582	1.24	7.91
			A = 8647.8 K^{-1} s^{-1}	975	0.86	—
		Orbach, direct (SR)	U_{eff} = 28.3 K, $\tau_0 = 2.46 \times 10^{-8}$ s, A = 682.6 K^{-1} s^{-1}			

maxima of Ir–Ln compounds were blue-shifted with respect to the parent metalloligand, which may be attributed to the deprotonation of the carboxylate groups upon coordination, leading to a decrease in the intermolecular H-bond interactions in the polymers.[36]

Further research on the photoluminescence efficiencies and time-resolved luminescence decay of the Ir^{III} unit and Ir–Ln compounds was carried out, and the data are summarized in Table 2. Owing to the mismatch in the energy levels, the Gd^{III} ions cannot accept energy from the triplet state of the Ir (III) unit,[37] so the photoluminescence efficiencies of **Ir_2Gd** and **Ir_4Gd_2** can be used as the reference for the other Ir–Ln (Ln = Dy, Yb, and Er) complexes. The quantum yield increases slightly from 4.22% to 5.83% (**Ir_2Gd**) and 8.08% (**Ir_4Gd_2**), which is attributed to the rigidity of the coordination framework that reduces self-quenching and the possibility of non-radiative transitions.[38] In addition, the long lifetime compared to the parent linker (6.60 μs) also implies that no d–f energy transfer occurs in **Ir_2Gd** and **Ir_4Gd_2** (Fig. S29†), while for the other luminescent Ir–Ln (Ln = Dy, Er, and Yb) coordination polymers, the lifetimes were shortened to varying degrees, which indicates that the energy effectively transfers from the light-harvesting Ir unit to the lanthanide centres. Moreover, according to the emission spectrum, the triplet energy level of $Ir(ppy)_2$(Hdcbpy) is 16 600 cm^{-1}, which is suitable for sensitizing the NIR lanthanide ions Yb^{III} and Er^{III}, but is too low to sensitize the low-lying excited state ($^4F_{9/2}$, 21 000 cm^{-1}) of Dy^{III} ions.[35,39]

In order to detect whether a lanthanide ion can be sensitized by the metalloligand $Ir(ppy)_2$(Hdcbpy), upon irradiation at 500 nm, the near-infrared emission spectra of Ir–Ln (Ln = Er and Yb) compounds were examined in the solid-state. For the Yb^{III} complexes, the emission bands occurring at 978 nm can be assigned to the $^2F_{5/2} \rightarrow {}^2F_{7/2}$ transition, while in **Ir_4Yb_2**, the emission peak shows a shoulder at 1005 nm, indicating that the local symmetry environment around the metal centre is affected by crystal-field splitting,[40] which is in agreement with the two independent Yb^{III} ions in the single crystal structure. The emission spectra of the Er^{III} complexes show an emission peak at around 1530 nm, which is attributed to the $^4I_{13/2} \rightarrow {}^4I_{15/2}$ transition.[41] Moreover, the luminescence decay is well fit to a bi-exponential curve, affording lifetimes of 0.92 μs for **Ir_2Yb**, 0.86 μs for **Ir_4Yb_2**, 1.40 μs for **Ir_2Er** and 1.37 μs for **Ir_4Er_2** (Fig. S30 and S31†). Noting that the quantum yields of **Ir_2Er** (ϕ = 0.68%) and **Ir_4Er_2** (ϕ = 1.08%) in the solid state are markedly lower than those of the other Ir–Ln (Ln = Gd, Dy, and Yb) complexes, the energy transfer between the metalloligand and erbium could be more efficient. This can be explained by the effective energy overlap between the ^{3}MLCT state of Ir $(ppy)_2$(Hdcbpy) and the f–f excited states of erbium.

Conclusion

In this work, we report a series of iridium(III)–lanthanide(III) bimetallic coordination polymers with single-chain (for **Ir_2Ln**) and double-chain (for **Ir_4Ln_2**) structures. Magnetic studies demonstrate that complexes **Ir_2Dy** and **Ir_4Dy_2** exhibit SMM behaviour in zero dc field, while complexes **Ir_2Er**, **Ir_2Yb**, **Ir_4Er_2** and **Ir_4Yb_2** show field-induced slow magnetic relaxation. The complex **Ir_4Yb_2** is of particular interest because of the field-induced dual relaxation processes, which may originate from the two different coordinated geometries of lanthanide ions. Moreover, in the complexes **Ir_2Er**, **Ir_2Yb**, **Ir_4Er_2** and **Ir_4Yb_2**, the Ir unit can act as a good light-harvesting antenna to effectively sensitize Ln-based near-infrared (NIR) luminescence by energy transfer from the Ir unit to the Ln^{3+} ions. As far as we know, this is the first observation of SMM behaviour and NIR luminescence coexisting in iridium(III)–lanthanide(III) bimetallic CPs.

Experimental section

Materials and physical measurements

All the starting materials were of reagent grade and were obtained from the commercial sources and used without further purification. Powder X-ray diffraction (PXRD) data were obtained using a Bruker D8 ADVANCE X-ray powder diffractometer (Cu-K_α) at room temperature. Infrared spectra were recorded on a Bruker Tensor 27 spectrometer using KBr pellets in the range of 400–4000 cm^{-1}. Thermogravimetric analysis (TGA) was performed under a nitrogen atmosphere in the temperature range of 25–600 °C at a heating rate of 5 °C min^{-1} using a METTLER TOLEDO TGA/DSC 1 instrument. Elemental analyses for C, H and N were performed with a PerkinElmer 240C elemental analyzer. The UV-vis spectra were recorded on a PerkinElmer Lambda 950 UV/Vis/NIR spectrometer using powder samples. The steady fluorescence spectra in the visible region were obtained using a PerkinElmer LS55 fluorescence spectrometer and a Xenon lamp as the excitation source. The emission lifetime and the absolute luminescent quantum yields in the solid state at room temperature were determined using a HORIBA FM-4P-TCSPC spectrometer. The steady state near infrared (NIR) emission spectra were recorded on an Edinburgh FLS980 fluorescence spectrometer equipped with a Hamamatsu R5509-72 photomultiplier. The magnetic susceptibility data were obtained using Quantum Design SQUID MPMS-XL7, VSM and PPMS magnetometer for freshly prepared samples. The diamagnetic contributions of the samples were estimated from Pascal's constants.

Synthesis of $[Ln\{Ir(ppy)_2(dcbpy)\}_2(NO_3)(H_2O)_n]\cdot$solvent ($Ir_2Ln$, n = 5, Ln = Gd and Dy; n = 4, Ln = Er and Yb)

Compounds **Ir_2Ln** (Ln = Gd, Dy, Er, and Yb) were synthesized under similar optimized experimental conditions. A typical procedure for the preparation of $[Yb\{Ir(ppy)_2(dcbpy)\}_2(NO_3)(H_2O)_4]\cdot 2CH_3OH\cdot 0.5H_2O$ (**Ir_2Yb**) is described below. Ir $(ppy)_2$(Hdcbpy) (7.4 mg, 0.01 mmol) was suspended in 2 mL of distilled water and dissolved in 5 μL of aqueous NaOH (1 M). Then $Yb(NO_3)_3\cdot 6H_2O$ (9.34 mg, 0.02 mmol) in 7 mL of MeOH was added. After keeping the vial at 60 °C for 2 days, orange rod crystals were obtained. The crystalline product of **Ir_2Yb** was

separated by filtration and washed with distilled water and a minimum amount of methanol. Yield: 29%. Elemental analyses (%) calcd for $C_{70}H_{61}YbIr_2N_9O_{17.5}$, C, 45.06; H, 3.29; N, 6.76; found: C, 45.09; H, 3.12; N, 6.74. IR (KBr, cm^{-1}): 3384 (m), 3105 (m), 3062 (m), 3043 (m), 1606 (s), 1585 (s), 1546 (m), 1477 (s), 1423 (s), 1380 (s), 1317 (w), 1288 (m), 1269 (m), 1234 (m), 1031 (w), 783 (m), 759 (s), 738 (w), 730 (w), 696 (w).

For $[Gd\{Ir(ppy)_2(dcbpy)\}_2(NO_3)(H_2O)_5]\cdot 2CH_3OH\cdot 0.5H_2O$ (**Ir_2Gd**): yield: 18%. Elemental analyses (%) calcd for $C_{70}H_{61}GdIr_2N_9O_{17.5}$, C, 45.45; H, 3.32; N, 6.81; found: C, 44.89; H, 3.27; N, 6.81. IR (KBr, cm^{-1}): 3355 (m), 3107 (w), 3059 (m), 2925 (m), 1631 (s), 1585 (s), 1544 (s), 1476 (s), 1421 (s), 1367 (s), 1270 (m), 1233 (m), 1160 (w), 864 (m), 781 (m), 758 (m), 694 (m), 670(w).

For $[Dy\{Ir(ppy)_2(dcbpy)\}_2(NO_3)(H_2O)_5]\cdot 2CH_3OH\cdot 0.5H_2O$ (**Ir_2Dy**): yield: 41%. Elemental analyses (%) calcd for $C_{70}H_{61}DyIr_2N_9O_{17.5}$, C, 45.32; H, 3.31; N, 6.79; found: C, 43.93; H, 3.26; N, 6.63. IR (KBr, cm^{-1}): 3423 (s), 3107 (w), 3049 (w), 1610 (s), 1546 (m), 1477 (s), 1427 (s), 1379 (s), 1313 (m), 1274 (m), 1234 (m), 1161 (w), 1062 (w), 1031 (w), 761 (m), 734 (w), 698 (w), 628 (w), 603 (w), 567 (w).

For $[Er\{Ir(ppy)_2(dcbpy)\}_2(NO_3)(H_2O)_4]\cdot 2CH_3OH\cdot 0.5H_2O$ (**Ir_2Er**): yield: 37%. Elemental analyses (%) calcd for $C_{70}H_{61}ErIr_2N_9O_{17.5}$, C, 45.20; H, 3.30; N, 6.77; found: C, 44.76; H, 3.24; N, 6.83. IR (KBr, cm^{-1}): 3375 (m), 3103 (m), 3043 (m), 1606 (s), 1585 (s), 1546 (m), 1514 (w), 1477 (s), 1421 (s), 1377 (s), 1286 (m), 1269 (m), 1232 (m), 1161 (w), 1031 (w), 781 (m), 759 (s), 738 (w), 729 (w), 696 (w).

Thermal analyses reveal that the weight losses at 90 °C are 4.2% (for **Ir_2Dy**), 4.4% (for **Ir_2Er**) and 3.9% (for **Ir_2Yb**) (Fig. S32†), which is in agreement with the release of lattice solvents (calcd 3.9% for $2CH_3OH + 0.5H_2O$). The weight loss for **Ir_2Gd** (5.6%) is higher than those for others, suggesting that one coordination water molecule could also be released below this temperature (calcd 4.9%). Between 90 and 300 °C slow weight losses occur corresponding to the partial removal of the coordination water molecule. Above 300 °C, the organic ligands start to decompose and the framework structures collapse.

Synthesis of $[Ln_2\{Ir(ppy)_2(dcbpy)\}_4(NO_3)_2(H_2O)_4]\cdot$solvent ($Ir_4Ln_2$; Ln = Gd, Dy, Er, and Yb)

Compounds **Ir_4Ln_2** (Ln = Gd, Dy, Er, and Yb) were synthesized under similar optimized experimental conditions. A typical preparation procedure for $[Yb_2(OH)\{Ir(ppy)_2(dcbpy)\}_4(NO_3)(H_2O)_4]\cdot 2CH_3OH\cdot 2.5H_2O$ (**Ir_4Yb_2**) is as follows. Ir(ppy)$_2$(Hdcbpy) (7.4 mg, 0.01 mmol) was suspended in 2 mL of distilled water and dissolved in 10 μL of aqueous NaOH (1 M). Then $Yb(NO_3)_3\cdot 6H_2O$ (9.34 mg, 0.02 mmol) in 7 mL of MeOH was added. An immediate precipitate of a green powder was obtained. After keeping the vial at 80 °C for 2 days, orange rod crystals were obtained. The crystalline product of **Ir_4Yb_2** was separated by filtration and washed with distilled water and a minimum amount of methanol. Yield: 23%. Elemental analyses (%) calcd for $C_{138}H_{110}N_{17}Yb_2Ir_4O_{28.5}$, C, 46.33; H, 3.10; N, 6.66; found: C, 45.82; H, 3.16; N, 6.83. IR (KBr, cm^{-1}): 3400 (s), 3103 (m), 3043 (m), 1608 (s), 1546 (m), 1477 (s), 1427 (s), 1379 (s), 1272 (w), 1232 (m), 1161 (w), 1031 (w), 866 (w), 784 (m), 761 (m), 734 (w), 698 (w), 630 (w).

For $[Gd_2(OH)\{Ir(ppy)_2(dcbpy)\}_4(NO_3)(H_2O)_4]\cdot 2CH_3OH\cdot 2.5H_2O$ (**Ir_4Gd_2**): yield: 15%. Elemental analyses (%) calcd for $C_{138}H_{110}N_{17}Gd_2Ir_4O_{28.5}$, C, 46.74; H, 3.13; N, 6.71; found: C, 45.97; H, 3.48; N, 6.99. IR (KBr, cm^{-1}): 3357 (s), 3105 (m), 3042 (m), 1604 (s), 1583 (s), 1562 (m), 1544 (s), 1476 (s), 1420 (s), 1365 (s), 1317 (m), 1269 (w), 1235 (m), 782 (m), 729 (w), 694 (w), 629 (w).

For $[Dy_2(OH)\{Ir(ppy)_2(dcbpy)\}_4(NO_3)(H_2O)_4]\cdot 2CH_3OH\cdot 2.5H_2O$ (**Ir_4Dy_2**): yield: 26%. Elemental analyses (%) calcd for $C_{138}H_{110}N_{17}Dy_2Ir_4O_{28.5}$, C, 46.61; H, 3.12; N, 6.70; found: C, 45.74; H, 3.21; N, 6.68. IR (KBr, cm^{-1}): 3429 (m), 3107 (m), 3053 (m), 1610 (s), 1548 (m), 1477 (s), 1425 (s), 1379 (s), 1271 (w), 1234 (w), 1162 (w), 1033 (w), 761 (s), 734 (w), 698 (w), 669 (w), 628 (w), 559 (w), 426 (w).

For $[Er_2(OH)\{Ir(ppy)_2(dcbpy)\}_4(NO_3)(H_2O)_4]\cdot 3CH_3OH\cdot 2.5H_2O$ (**Ir_4Er_2**): yield: 28%. Elemental analyses (%) calcd For $C_{139}H_{114}N_{17}Er_2Ir_4O_{29.5}$, C, 46.40; H, 3.19; N, 6.62; found: C, 45.50; H, 3.57; N, 6.48. IR (KBr, cm^{-1}): 3402 (m), 3107 (m), 3045 (m), 1608 (s), 1546 (m), 1477 (s), 1427 (s), 1380 (s), 1271 (w), 1234 (w), 1161 (w), 1031 (w), 784 (m), 761 (m), 734 (w), 698 (w), 630 (w).

Thermal analyses reveal that the weight losses at 100 °C are 2.8% for **Ir_4Gd_2**, **Ir_4Dy_2** and **Ir_4Yb_2** (Fig. S33†), which is in agreement with the release of two CH_3OH and $2.5H_2O$ molecules (calcd 3.0–3.1%). The weight loss for **Ir_4Er_2** is 4.1%, corresponding to the release of three CH_3OH and 2.5 H_2O molecules (calcd 3.9%). The number of solvent molecules for **Ir_4Yb_2** is less than that obtained from the single crystal structural determination, suggesting that the lattice solvents are partially released at room temperature. The weight losses between 100 and 300 °C are attributed to the partial release of the coordination water molecules, and above 300 °C the structure begins to collapse.

X-ray crystallographic analyses

Suitable single crystals were selected for indexing and obtaining intensity data using a Bruker SMART APEX D8 diffractometer equipped with a graphite-monochromated Mo Kα radiation source (λ = 0.71073 Å) at 150 K.[42] Adsorption corrections were carefully performed for all data. The structures were solved by direct methods and refined on F^2 by full-matrix least squares using SHELXTL.[43] All non-hydrogen atoms were located in the Fourier maps and were refined with anisotropic thermal parameters. All H atoms were either placed in the calculated positions or found in the F-maps and refined isotropically.

In the case of **Ir_2Dy**, the residual electron densities in the solvent-accessible void due to heavily disordered solvent molecules and nitrate anions were determined using the PLATON/SQUEEZE program.[44] In cases of **Ir_2Er**, **Ir_2Yb** and **Ir_4Yb_2**, the lattice solvent molecules and nitrate anions were found in the Fourier map. The hydrogen atoms of disordered water molecules were not placed. Quite large (2.2–5.3 e A^3) residual elec-

tron density peaks were located near the Ln or Ir atoms in the corresponding structures, and could not be reasonably modelled with the disordered atoms. The crystallographic data and refinement details are listed in Table 1. The selected bond lengths and angles for **Ir_2Dy**, **Ir_2Er**, **Ir_2Yb** and **Ir_4Yb_2** are given in Tables S1–S7.†

Conflicts of interest

There are no conflicts to declare.

Acknowledgements

Financial support from the National Key R&D Program of China (2017YFA0303203, 2018YFA0306004) and the National Natural Science Foundation of China (21731003) is acknowledged. MK is funded by the CNRS (France).

Notes and references

1 (*a*) Y. Cui, B. Li, H. He, W. Zhou, B. Chen and G. Qian, Metal-Organic Frameworks as Platforms for Functional Materials, *Acc. Chem. Res.*, 2016, **49**, 483–493; (*b*) S. Roy, A. Chakraborty and T. K. Maji, Lanthanide-organic frameworks for gas storage and as magneto-luminescent materials, *Coord. Chem. Rev.*, 2014, **273–274**, 139–164; (*c*) Y.-S. Meng and T. Liu, Manipulating Spin Transition To Achieve Switchable Multifunctions, *Acc. Chem. Res.*, 2019, **52**, 1369–1379.

2 (*a*) J. Long, Y. Guari, R. A. S. Ferreira, L. D. Carlos and J. Larionova, Recent advances in luminescent lanthanide based Single-Molecule Magnets, *Coord. Chem. Rev.*, 2018, **363**, 57–70; (*b*) J.-H. Jia, Q.-W. Li, Y.-C. Chen, J.-L. Liu and M.-L. Tong, Luminescent single-molecule magnets based on lanthanides: Design strategies, recent advances and magneto-luminescent studies, *Coord. Chem. Rev.*, 2019, **378**, 365–381; (*c*) F. Pointillart, B. le Guennic, O. Cador, O. Maury and L. Ouahab, Lanthanide Ion and Tetrathiafulvalene-Based Ligand as a "Magic" Couple toward Luminescence, Single Molecule Magnets, and Magnetostructural Correlations, *Acc. Chem. Res.*, 2015, **48**, 2834–2842.

3 (*a*) M. M. Paquette, D. Plaul, A. Kurimoto, B. O. Patrick and N. L. Frank, Opto-Spintronics: Photoisomerization-Induced Spin State Switching at 300 K in Photochrome Cobalt-Dioxolene Thin Films, *J. Am. Chem. Soc.*, 2018, **140**, 14990–15000; (*b*) J.-L. Wang, Q. Liu, Y.-S. Meng, X. Liu, H. Zheng, Q. Shi, C.-Y. Duan and T. Liu, Fluorescence modulation *via* photoinduced spin crossover switched energy transfer from fluorophores to Fe^{II} ions, *Chem. Sci.*, 2018, **9**, 2892–2897; (*c*) M. Estrader, J. S. Uber, L. A. Barrios, J. Garcia, P. Lloyd-Williams, O. Roubeau, S. J. Teat and G. Aromí, A Magneto-optical Molecular Device: Interplay of Spin Crossover, Luminescence, Photomagnetism, and Photochromism, *Angew. Chem., Int. Ed.*, 2017, **56**, 15622–15627; (*d*) T. Delgado, M. Meneses-Sánchez, L. Piñeiro-López, C. Bartual-Murgui, M. C. Muñoz and J. A. Real, Thermo- and photo-modulation of exciplex fluorescence in a 3D spin crossover Hofmann-type coordination polymer, *Chem. Sci.*, 2018, **9**, 8446–8452; (*e*) X.-D. Huang, M. Kurmoo, S.-S. Bao, K. Fan, Y. Xu, Z.-B. Hu and L.-M. Zheng, Coupling photo-, mechano- and thermochromism and single-ion-magnetism of two mononuclear dysprosium-anthracene-phosphonate complexes, *Chem. Commun.*, 2018, **54**, 3278–3281; (*f*) J. Yuan, S.-Q. Wu, M.-J. Liu, O. Sato and H.-Z. Kou, Rhodamine 6G-Labeled Pyridyl Aroylhydrazone Fe(II) Complex Exhibiting Synergetic Spin Crossover and Fluorescence, *J. Am. Chem. Soc.*, 2018, **140**, 9426–9433.

4 (*a*) B. M. Day, F.-S. Guo and R. A. Layfield, Cyclopentadienyl Ligands in Lanthanide Single-Molecule Magnets: One Ring To Rule Them All?, *Acc. Chem. Res.*, 2018, **51**, 1880–1889; (*b*) M. Ren and L.-M. Zheng, Lanthanide-based Single Molecule Magnets, *Acta Chim. Sin.*, 2015, **73**, 1091–1113; (*c*) Z.-H. Zhu, M. Guo, X.-L. Li and J.-K. Tang, Molecular magnetism of lanthanide: Advances and perspectives, *Coord. Chem. Rev.*, 2019, **378**, 350–364.

5 (*a*) Y.-S. Meng, S.-D. Jiang, B.-W. Wang and S. Gao, Understanding the Magnetic Anisotropy toward Single-Ion Magnets, *Acc. Chem. Res.*, 2016, **49**, 2381–2389; (*b*) D. N. Woodruff, R. E. P. Winpenny and R. A. Layfield, Lanthanide Single-Molecule Magnets, *Chem. Rev.*, 2013, **113**, 5110–5148; (*c*) K. Liu, X.-J. Zhang, X.-X. Meng, W. Shi, P. Cheng and A. K. Powell, Constraining the coordination geometries of lanthanide centers and magnetic building blocks in frameworks: a new strategy for molecular nanomagnets, *Chem. Soc. Rev.*, 2016, **45**, 2423–2439; (*d*) H.-L. Wang, B.-W. Wang, Y.-Z. Bian, S. Gao and J.-Z. Jiang, Single-molecule magnetism of tetrapyrrole lanthanide compounds with sandwich multiple-decker structures, *Coord. Chem. Rev.*, 2016, **306**, 195–216; (*e*) F.-S. Guo, B. M. Day, Y.-C. Chen, M.-L. Tong, A. Mansikkamäki and R. A. Layfield, Magnetic hysteresis up to 80 kelvin in a dysprosium metallocene single-molecule magnet, *Science*, 2018, **362**, 1400–1403.

6 J. G. Bünzli, On the design of highly luminescent lanthanide complexes, *Coord. Chem. Rev.*, 2015, **293–294**, 19–47.

7 (*a*) M. Pan, W.-M. Liao, S.-Y. Yin, S.-S. Sun and C.-Y. Su, Single-Phase White-Light-Emitting and Photoluminescent Color-Tuning Coordination Assemblies, *Chem. Rev.*, 2018, **118**, 8889–8935; (*b*) Y. Hasegawa and Y. Kitagawa, Thermosensitive luminescence of lanthanide complexes, clusters, coordination polymers and metal-organic frameworks with organic photosensitizers, *J. Mater. Chem. C*, 2019, **7**, 7494–7511.

8 (*a*) A. T. Bui, A. Roux, A. Grichine, A. Duperray, C. Andraud and O. Maury, Twisted Charge-Transfer Antennae for Ultra-Bright Terbium(III) and Dysprosium(III) Bioprobes, *Chem. – Eur. J.*, 2018, **24**, 3408–3412; (*b*) D. Kovacs, D. Phipps,

A. Orthaber and K. E. Borbas, Highly luminescent lanthanide complexes sensitised by tertiary amide-linked carbostyril antennae, *Dalton Trans.*, 2018, **47**, 10702–10714; (*c*) M. Ren, Z.-L. Xu, S.-S. Bao, T.-T. Wang, Z.-H. Zheng, R. A. Ferreira, L.-M. Zheng and L. D. Carlos, Lanthanide salen-type complexes exhibiting single ion magnet and photoluminescent properties, *Dalton Trans.*, 2016, **45**, 2974–2982; (*d*) Y. Ning, X.-S. Ke, J.-Y. Hu, Y.-W. Liu, F. Ma, H.-L. Sun and J.-L. Zhang, Bioinspired Orientation of β-Substituents on Porphyrin Antenna Ligands Switches Ytterbium(III) NIR Emission with Thermosensitivity, *Inorg. Chem.*, 2017, **56**, 1897–1905; (*e*) B. S. K. Chong and E. G. Moore, Quantitative Sensitization Efficiencies in NIR-Emissive Homoleptic Ln(III) Complexes Using 2-(5-Methylpyridin-2-yl)-8-hydroxyquinoline, *Inorg. Chem.*, 2018, **57**, 14062–14072; (*f*) Q. Zou, X.-D. Huang, J. C. Liu, S.-S. Bao and L.-M. Zheng, Lanthanide anthracene complexes: slow magnetic relaxation and luminescence in Dy^{III}, Er^{III} and Yb^{III} based materials, *Dalton Trans.*, 2019, **48**, 2735–2740.

9 F.-F. Chen, Z.-Q. Chen, Z.-Q. Bian and C.-H. Huang, Sensitized luminescence from lanthanides in d–f bimetallic complexes, *Coord. Chem. Rev.*, 2010, **254**, 991–1010.

10 (*a*) C. Giansante, P. Ceroni, V. Balzani and F. Vögtle, Self-Assembly of a Light-Harvesting Antenna Formed by a Dendrimer, a Ru^{II} Complex, and a Nd^{III} Ion, *Angew. Chem., Int. Ed.*, 2008, **47**, 5422–5425; (*b*) H.-B. Xu, X.-L. Chen, J.-G. Deng, Z.-H. Deng, S.-L. Huang, M. Kurmoo and M.-H. Zeng, Sensitized near infrared emission through supramolecular d → f energy transfer within an ionic Ru(II)-Er(III) pair, *Dalton Trans.*, 2018, **47**, 2073–2078.

11 (*a*) Y. You and W. Nam, Photofunctional triplet excited states of cyclometalated Ir(III) complexes: beyond electroluminescence, *Chem. Soc. Rev.*, 2012, **41**, 7061–7084; (*b*) D. R. Martir and E. Zysman-Colman, Supramolecular iridium(III) assemblies, *Coord. Chem. Rev.*, 2018, **364**, 86–117.

12 M. Mehlstäubl, G. S. Kottas, S. Colella and L. De Cola, Sensitized near-infrared emission from ytterbium(III) via direct energy transfer from iridium(III) in a heterometallic neutral complex, *Dalton Trans.*, 2008, 2385–2388.

13 (*a*) F. Chen, Z. Bian, B. Lou, E. Ma, Z. Liu, D. Nie, Z. Chen, J. Bian, Z. Chen and C. Huang, Sensitised near-infrared emission from lanthanides using an iridium complex as a ligand in heteronuclear Ir_2Ln arrays, *Dalton Trans.*, 2008, 5577–5583; (*b*) F. Chen, Z. Bian, Z. Liu, D. Nie, Z. Chen and C. Huang, Highly Efficient Sensitized Red Emission from Europium(III) in Ir-Eu Bimetallic Complexes by ^{3}MLCT Energy Transfer, *Inorg. Chem.*, 2008, **47**, 2507–2513; (*c*) L.-Y. Zhang, Y.-J. Hou, M. Pan, L. Chen, Y.-X. Zhu, S.-Y. Yin, G. Shao and C.-Y. Su, Near-infrared (NIR) emitting Nd/Yb(III) complexes sensitized by MLCT states of Ru(II)/Ir(III) metalloligands in the visible light region, *Dalton Trans.*, 2015, **44**, 15212–15219; (*d*) F.-F. Chen, H.-B. Wei, Z.-Q. Bian, Z.-W. Liu, E. Ma, Z.-N. Chen and C.-H. Huang, Sensitized Near-Infrared Emission from Ir-III-Ln(III) (Ln = Nd, Yb, Er) Bimetallic Complexes with a ((NO)-O-boolean AND)((NO)-O-boolean AND) Bridging Ligand, *Organometallics*, 2014, **33**, 3275–3282; (*e*) A. Jana, S. J. A. Pope and M. D. Ward, D → f energy transfer in heteronuclear Ir(III)/Ln(III) near-infrared luminescent complexes, *Polyhedron*, 2017, **127**, 390–395.

14 L. Li, S. Zhang, L. Xu, Z.-N. Chen and J. Luo, Highly sensitized near-infrared luminescence in Ir-Ln heteronuclear coordination polymers via light-harvesting antenna of Ir(III) unit, *J. Mater. Chem. C*, 2014, **2**, 1698–1703.

15 (*a*) D. Zeng, M. Ren, S.-S. Bao, L. Li and L.-M. Zheng, A luminescent heptanuclear $DyIr_6$ complex showing field-induced slow magnetization relaxation, *Chem. Commun.*, 2014, **50**, 8356–8359; (*b*) D. Zeng, K. Fan, L.-P. Wang, S.-S. Bao, M. Ren and L.-M. Zheng, Octahedral erbium and ytterbium ion encapsulated in phosphorescent iridium complexes showing field-induced magnetization relaxation, *J. Magn. Magn. Mater.*, 2019, **484**, 139–145.

16 (*a*) X.-D. Huang, Y. Xu, K. Fan, S.-S. Bao, M. Kurmoo and L.-M. Zheng, Reversible SC-SC Transformation involving [4 + 4] Cycloaddition of Anthracene: A Single-Ion to Single-Molecule Magnet and Yellow-Green to Blue-White Emission, *Angew. Chem., Int. Ed.*, 2018, **57**, 8577–8581; (*b*) X.-D. Huang, J.-G. Jia, M. Kurmoo, S.-S. Bao and L.-M. Zheng, Interplay of anthracene luminescence and dysprosium magnetism by steric control of photodimerization, *Dalton Trans.*, 2019, **48**, 13769–13779.

17 (*a*) M. Pinsky and D. Avnir, Continuous Symmetry Measures. 5. The Classical Polyhedra, *Inorg. Chem.*, 1998, **37**, 5575–5582; (*b*) D. Casanova, P. Alemany, J. M. Bofill and S. Alvarez, Shape and Symmetry of Heptacoordinate Transition-Metal Complexes: Structural Trends, *Chem. – Eur. J.*, 2003, **9**, 1281–1295.

18 L. Li, S. Zhang, L. Xu, J. Wang, L. Shi, Z. Chen, M. Hong and J. Luo, Effective visible-light driven CO_2 photoreduction *via* a promising bifunctional iridium coordination polymer, *Chem. Sci.*, 2014, **5**, 3808–3813.

19 (*a*) L. Norel, L. E. Darago, B. L. Guennic, K. Chakarawet, M. I. Gonzalez, J. H. Olshansky, S. Rigaut and J. R. Long, A Terminal Fluoride Ligand Generates Axial Magnetic Anisotropy in Dysprosium Complexes, *Angew. Chem., Int. Ed.*, 2018, **57**, 1933–1938; (*b*) E. Moreno-Pineda, G. Taran, W. Wernsdorfer and M. Ruben, Quantum tunnelling of the magnetisation in single-molecule magnet isotopologue dimers, *Chem. Sci.*, 2019, **10**, 5138–5145.

20 X.-J. Zhang, S. Liu, V. Vieru, N. Xu, C. Gao, B.-W. Wang, W. Shi, L. F. Chibotaru, S. Gao, P. Cheng and A. K. Powell, Coupling Influences SMM Properties for Pure 4 f Systems, *Chem. – Eur. J.*, 2018, **24**, 6079–6086.

21 K. L. M. Harriman, J. J. Le Roy, L. Ungur, R. J. Holmberg, I. Korobkova and M. Murugesu, Cycloheptatrienyl trianion: an elusive bridge in the search of exchange coupled dinuclear organolanthanide single-molecule magnets, *Chem. Sci.*, 2017, **8**, 231–240.

22 (*a*) K. S. Cole and R. H. Cole, Dispersion and absorption in dielectrics: Alternating current characteristics, *J. Chem.*

Phys., 1941, **9**, 341–351; (*b*) Y.-N. Guo, G.-F. Xu, Y. Guo and J.-K. Tang, Relaxation dynamics of dysprosium(III) single molecule magnets, *Dalton Trans.*, 2011, **40**, 9953–9963; (*c*) N. F. Chilton, *CC-Fit*, The University of Manchester, Manchester, UK, 2014, http://www.nfchilton.com/cc-fit.html.

23 (*a*) S.-M. Chen, J. Xiong, Y.-Q. Zhang, Q. Yuan, B.-W. Wang and S. Gao, A soft phosphorus atom to "harden" an erbium (III) single-ion magnet, *Chem. Sci.*, 2018, **9**, 7540–7545; (*b*) K. Katoh, S. Yamashita, N. Yasuda, Y. Kitagawa, B. K. Breedlove, Y. Nakazawa and M. Yamashita, Control of the Spin Dynamics of Single-Molecule Magnets by using a Quasi One-Dimensional Arrangement, *Angew. Chem., Int. Ed.*, 2018, **57**, 9262–9267.

24 (*a*) J.-J. Lu, Y.-Q. Zhang, X.-L. Li, M. Guo, J.-F. Wu, L. Zhao and J.-K. Tang, Influence of Magnetic Interactions and Single-Ion Anisotropy on Magnetic Relaxation within a Family of Tetranuclear Dysprosium Complexes, *Inorg. Chem.*, 2019, **58**, 5715–5724; (*b*) R. Boča, C. Rajnák, J. Titiš and D. Valigura, Field Supported Slow Magnetic Relaxation in a Mononuclear Cu(II) Complex, *Inorg. Chem.*, 2017, **56**, 1478–1482.

25 (*a*) C. Schlesier, L. Spree, A. Kostanyan, R. Westerström, A. Brandenburg, A. U. B. Wolter, S.-F. Yang, T. Greber and A. A. Popov, Strong carbon cage influence on the single molecule magnetism in Dy-Sc nitride clusterfullerenes, *Chem. Commun.*, 2018, **54**, 9730–9733; (*b*) H.-L. Gao, S.-X. Huang, X.-P. Zhou, Z. Liu and J.-Z. Cui, Magnetic properties and structure of tetranuclear lanthanide complexes based on 8-hydroxylquinoline Schiff base derivative and β-diketone coligand, *Dalton Trans.*, 2018, **47**, 3503–3511.

26 (*a*) J. Vallejo, J. Cano, I. Castro, M. Julve, F. Lloret, O. Fabelo, L. Cañadillas-Delgado and E. Pardo, Slow magnetic relaxation in carbonato-bridged dinuclear lanthanide (III) complexes with 2,3-quinoxalinediolate ligands, *Chem. Commun.*, 2012, **48**, 7726–7728; (*b*) K. L. M. Harriman and M. Murugesu, An Organolanthanide Building Block Approach to Single-Molecule Magnets, *Acc. Chem. Res.*, 2016, **49**, 1158–1167.

27 K. Kumar, O. Stefanczyk, S. Chorazy, K. Nakabayashi, B. Sieklucka and S.-i. Ohkoshi, Effect of Noble Metals on Luminescence and Single-Molecule Magnet Behavior in the Cyanido-Bridged Ln-Ag and Ln-Au (Ln = Dy, Yb, Er) Complexes, *Inorg. Chem.*, 2019, **58**, 5677–5687.

28 (*a*) Y.-Q. Zhai, Y.-F. Deng and Y.-Z. Zheng, Pseudotetrahedral cobalt(II) complexes with PNP-ligands showing uniaxial magnetic anisotropy, *Dalton Trans.*, 2018, **47**, 8874–8878; (*b*) J. Li, S. Gomez-Cocá, B. S. Dolinar, L. Yang, F. Yu, M. Kong, Y.-Q. Zhang, Y. Song and K. R. Dunbar, Hexagonal Bipyramidal Dy(III) Complexes as a Structural Archetype for Single-Molecule Magnets, *Inorg. Chem.*, 2019, **58**, 2610–2617.

29 (*a*) L. Mandal, S. Biswas, G. Cosquer, Y.-B. Shen and M. Yamashita, Anion-driven structures and SMM behavior of dinuclear terbium and ytterbium complexes, *Dalton Trans.*, 2018, **47**, 17493–17499; (*b*) H.-Q. Tian, B.-L. Wang, J. Lu, H.-T. Liu, J.-H. Su, D.-C. Li and J.-M. Dou, Consecutive one-/two-step relaxation transformations of single-molecule magnets via coupling dinuclear dysprosium compounds with chloride bridges, *Chem. Commun.*, 2018, **54**, 12105–12108.

30 (*a*) S. G. McAdams, A. Ariciu, A. K. Kostopoulos, J. P. S. Walsh and F. Tuna, Molecular single-ion magnets based on lanthanides and actinides: Design considerations and new advances in the context of quantum technologies, *Coord. Chem. Rev.*, 2017, **346**, 216–239; (*b*) J.-L. Liu, Y.-C. Chen and M.-L. Tong, Symmetry strategies for high performance lanthanide-based single-molecule magnets, *Chem. Soc. Rev.*, 2018, **47**, 2431–2453.

31 (*a*) J.-L. Liu, Y.-C. Chen, Y.-Z. Zheng, W.-Q. Lin, L. Ungur, W. Wernsdorfer, L. F. Chibotaru and M.-L. Tong, Switching the anisotropy barrier of a single-ion magnet by symmetry change from quasi-D_{5h} to quasi-O_h, *Chem. Sci.*, 2013, **4**, 3310–3316; (*b*) J. Liu, Y.-C. Chen, J.-L. Liu, V. Vieru, L. Ungur, J. Jia, L. F. Chibotaru, Y.-H. Lan, W. Wernsdorfer, S. Gao, X.-M. Chen and M.-L. Tong, A Stable Pentagonal Bipyramidal Dy(III) Single-Ion Magnet with a Record Magnetization Reversal Barrier over 1000 K, *J. Am. Chem. Soc.*, 2016, **138**, 5441–5450; (*c*) Y.-C. Chen, J.-L. Liu, W. Wernsdorfer, D. Liu, L. F. Chibotaru, X.-M. Chen and M.-L. Tong, Hyperfine-Interaction-Driven Suppression of Quantum Tunneling at Zero Field in a Holmium(III) Single-Ion Magnet, *Angew. Chem., Int. Ed.*, 2017, **56**, 4996–5000.

32 (*a*) Y.-S. Ding, N. F. Chilton, R. E. P. Winpenny and Y.-Z. Zheng, On Approaching the Limit of Molecular Magnetic Anisotropy: A Near-Perfect Pentagonal Bipyramidal Dysprosium(III) Single-Molecule Magnet, *Angew. Chem., Int. Ed.*, 2016, **55**, 16071–16074; (*b*) L. Ungur and L. F. Chibotaru, Strategies toward High-Temperature Lanthanide-Based Single-Molecule Magnets, *Inorg. Chem.*, 2016, **55**, 10043–10056; (*c*) S. K. Gupta, T. Rajeshkumar, G. Rajaraman and R. Murugavel, An air-stable Dy(III) single-ion magnet with high anisotropy barrier and blocking temperature, *Chem. Sci.*, 2016, **7**, 5181–5191.

33 (*a*) J. D. Rinehart and J. R. Long, Exploiting single-ion anisotropy in the design of f-element single-molecule magnets, *Chem. Sci.*, 2011, **2**, 2078–2085; (*b*) M. Ren, S.-S. Bao, B.-W. Wang, R. A. S. Ferreira, L.-M. Zheng and L. D. Carlos, Lanthanide phosphonates with pseudo-D_{5h} local symmetry exhibiting magnetic and luminescence bifunctional properties, *Inorg. Chem. Front.*, 2015, **2**, 558–566; (*c*) M. Ren, S.-S. Bao, R. A. S. Ferreira, L.-M. Zheng and L. D. Carlos, A layered erbium phosphonate in pseudo-D_{5h} symmetry exhibiting field-tunable magnetic relaxation and optical correlation, *Chem. Commun.*, 2014, **50**, 7621–7624; (*d*) X.-C. Huang, M. Zhang, D. Wu, D. Shao, X.-H. Zhao, W. Huang and X.-Y. Wang, Single molecule magnet behavior observed in a 1-D dysprosium chain with quasi-D_{5h} symmetry, *Dalton Trans.*, 2015, **44**, 20834–20838; (*e*) J. Long, A. N. Selikhov, E. Mamontova, K. A. Lyssenko, Y. Guari, J. Larionova and A. A. Trifonov, Single-molecule magnet

behaviour in a Dy(III) pentagonal bipyramidal complex with a quasi-linear Cl-Dy-Cl sequence, *Dalton Trans.*, 2019, **48**, 35–39; (*f*) M. Li, H. Wu, Q. Yang, H. Ke, B. Yin, Q. Shi, W. Wang, Q. Wei, G. Xie and S. Chen, Experimental and Theoretical Interpretation on the Magnetic Behavior in a Series of Pentagonal-Bipyramidal Dy^{III} Single-Ion Magnets, *Chem. – Eur. J.*, 2017, **23**, 17775–17787.

34 S. Lamansky, P. Djurovich, D. Murphy, F. Abdel-Razzaq, R. Kwong, I. Tsyba, M. Bortz, B. Mui, R. Bau and M. E. Thompson, Synthesis and Characterization of Phosphorescent Cyclometalated Iridium Complexes, *Inorg. Chem.*, 2001, **40**, 1704–1711.

35 W. T. Carnall, P. R. Fields and K. Rajnak, Electronic Energy Levels in the Trivalent Lanthanide Aquo Ions. I. Pr^{3+}, Nd^{3+}, Pm^{3+}, Sm^{3+}, Dy^{3+}, Ho^{3+}, Er^{3+}, and Tm^{3+}, *J. Chem. Phys.*, 1968, **49**, 4424–4442.

36 (*a*) J. B. Waern, C. Desmarets, L. Chamoreau, H. Amouri, A. Barbieri, C. Sabatini, B. Ventura and F. Barigelletti, Luminescent Cyclometalated Rh^{III}, Ir^{III}, and $(DIP)_2Ru^{II}$ Complexes with Carboxylated Bipyridyl Ligands: Synthesis, X-ray Molecular Structure, and Photophysical Properties, *Inorg. Chem.*, 2008, **47**, 3340–3348; (*b*) W. Jiang, Y. Gao, Y. Sun, F. Ding, Y. Xu, Z. Bian, F. Li, J. Bian and C. Huang, Zwitterionic Iridium Complexes: Synthesis, Luminescent Properties, and Their Application in Cell Imaging, *Inorg. Chem.*, 2010, **49**, 3252–3260; (*c*) M. Ho, Y. Chen, T. Chen, P. Chang, Y. Yu, K. Cheng, C. Shih, G. Lee and H. Sheu, Synthesis, structure and oxygen-sensing properties of Iridium(III)-containing coordination polymers with different cations, *Dalton Trans.*, 2012, **41**, 2592–2600; (*d*) L. Li, S. Zhang, L. Xu, L. Han, Z. Chen and J. Luo, An Intensely Luminescent Metal-Organic Framework Based on a Highly Light-Harvesting Dyclo-Metalated Iridium(III) Unit Showing Effective Detection of Explosives, *Inorg. Chem.*, 2013, **52**, 12323–12325.

37 (*a*) W. T. Carnall, P. R. Fields and K. Rajnak, Spectral Intensities of the Trivalent Lanthanides and Actinides in Solution. II. Pm^{3+}, Sm^{3+}, Eu^{3+}, Gd^{3+}, Tb^{3+}, Dy^{3+}, and Ho^{3+}, *J. Chem. Phys.*, 1968, **49**, 4412–4423; (*b*) D. Sykes and M. D. Ward, Visible-light sensitisation of Tb(III) luminescence using a blue-emitting Ir(III) complex as energy-donor, *Chem. Commun.*, 2011, **47**, 2279–2281; (*c*) A. Jana, B. J. Crowston, J. R. Shewring, L. K. McKenzie, H. E. Bryant, S. W. Botchway, A. D. Ward, A. J. Amoroso, E. Baggaley and M. D. Ward, Heteronuclear Ir(III)–Ln(III) Luminescent Complexes: Small-Molecule Probes for Dual Modal Imaging and Oxygen Sensing, *Inorg. Chem.*, 2016, **55**, 5623–5633.

38 (*a*) Y. Wang, T. Yang, X. Liu, G. Li, W. Che, D. Zhu and Z. Su, New cationic Ir(III) complexes without "any soft substituents": aggregation-induced emission and piezochromic luminescence, *J. Mater. Chem. C*, 2018, **6**, 12217–12223; (*b*) D. G. Congrave, Y.-T. Hsu, A. S. Batsanov, A. Beeby and M. R. Bryce, Sky-blue emitting bridged diiridium complexes: beneficial effects of intramolecular π–π stacking, *Dalton Trans.*, 2018, **47**, 2086–2098; (*c*) L. He, D. Ma, L. Duan, Y. Wei, J. Qiao, D. Zhang, G. Dong, L. Wang and Y. Qiu, Control of Intramolecular π–π Stacking Interaction in Cationic Iridium Complexes via Fluorination of Pendant Phenyl Rings, *Inorg. Chem.*, 2012, **51**, 4502–4510.

39 (*a*) E. G. Moore, A. P. S. Samuel and K. N. Raymond, From Antenna to Assay: Lessons Learned in Lanthanide Luminescence, *Acc. Chem. Res.*, 2009, **42**, 542–552; (*b*) S. V. Eliseeva and J. G. Buenzli, Lanthanide luminescence for functional materials and bio-sciences, *Chem. Soc. Rev.*, 2010, **39**, 189–227.

40 (*a*) D. Li, F.-F. Chen, Z.-Q. Bian, Z.-W. Liu, Y.-L. Zhao and C.-H. Huang, Sensitized near-infrared emission of Yb^{III} from an Ir^{III}–Yb^{III} bimetallic complex, *Polyhedron*, 2009, **28**, 897–902; (*b*) J. E. Jones, R. L. Jenkins, R. S. Hicks, A. J. Hallett and S. J. A. Pope, Water-soluble, luminescent iridium(III)-ytterbium(III) complexes using dipyrido[3,2-a:2′,3′-c]phenazine derivatives as bridging units, *Dalton Trans.*, 2012, **41**, 10372–10381.

41 (*a*) J. G. Bünzli and S. V. Eliseeva, Lanthanide NIR luminescence for telecommunications, bioanalyses and solar energy conversion, *J. Rare Earths*, 2010, **28**, 824–842; (*b*) Y. Xu, S.-S. Bao, X.-D. Huang and L.-M. Zheng, Homochiral Erbium Coordination Polymers: Salt-Assisted Conversion from Triple to Quadruple Helices, *Cryst. Growth Des.*, 2018, **18**, 4045–4053.

42 *SAINT, Program for Data Extraction and Reduction*, Siemens Analytical X-ray Instruments, Madison, WI, 1994–1996.

43 *SHELXTL (version 5.0), Reference Manual, Siemens Industrial Automation*, Analytical Instruments, Madison, WI, 1995.

44 A. L. Spek, Single-crystal structure validation with the program PLATON, *J. Appl. Crystallogr.*, 2003, **36**, 7–13.

